Journal of Infrared, Millimeter, and Terahertz Waves
https://doi.org/10.1007/s10762-023-00918-1

# Terahertz Beam Steering with Curved Metasurfaces

**Yaseman Shiri**[1] · **Hichem Guerboukha**[1] · **Daniel M. Mittleman**[1]

Received: 7 March 2023 / Accepted: 27 April 2023


**Abstract**
Considerable recent research interest has focused on the possibility of using metasurfaces for manipulation of terahertz wavefronts. For example, metasurfaces allow a beam to be targeted in any desired direction using strategically placed meta-elements. With rapid prototyping techniques, metasurfaces can be fabricated quickly and at a low cost. These techniques also permit the fabrication of metasurfaces on flexible substrates which can be bent easily. This opens the possibility of employing such devices as conformable arrays on non-flat surfaces. To explore this idea, we experimentally and numerically analyze the performance of a terahertz metasurface printed on paper, as a function of its radius of curvature. We observe that when the metasurface is bent, the direction of the refracted beam is minimally impacted and the performance of the metasurface remains very similar to when it is flat. This conclusion will simplify the design and modeling criteria for conformable metasurfaces.

**Keywords** Terahertz · Terahertz communications · Metasurfaces · Beamsteering · Beamforming · Conformal metasurface

## 1 Introduction

Wireless communications at frequencies above 100 GHz have become a focus of research for future societal needs. As carrier frequencies increase from RF range to the THz range, the smaller sizes of the antennas can prove to be efficient and beneficial [1–4]. On the other hand, this shift in frequency also poses a number of challenges. Atmospheric absorption and free-space path loss can limit transmission distances at these higher frequencies [5–8]. One way to improve the performance of wireless systems in the face of this challenge is by using terahertz wavefront shaping to direct and steer the terahertz beam. Beamforming and beam steering are also important capabilities in secure wireless communications to avoid eavesdroppers and other malicious agents [9, 10]. In this context, metasurfaces have been

✉ Yaseman Shiri
yaseman_shiri@brown.edu

[1] School of Engineering, Brown University, Providence, RI 02912, USA

Published online: 15 May 2023

proposed as a versatile platform to realize wavefront engineering in this spectral range [11–13]. These devices are composed of arrays of subwavelength structures that can vary in geometry, commonly referred to as "meta-atoms." By judicious geometrical engineering, these meta-atoms can be arranged such that the array realizes a given amplitude and phase response in transmission and/or reflection, at a given frequency.

Researchers have studied many different geometrical configurations of meta-atoms. These metallic elements, with dimensions of typically λ/5 or smaller, must be deposited on a transparent low-loss substrate. The ability to develop these metasurfaces using various fabrication techniques, such as lithography and laser ablation [14], allows for a wide variety of substrate and metallic or dielectric combinations. The possibility to control phase and amplitude makes metasurfaces ideal for wavefront shaping applications such as beam steering and meta-lenses [15]. For beam forming, an engineered phase gradient can be used to steer the direction of the beam, depending on the arrangement and geometrical pattern of the unit structures. Metamaterials have been realized in the terahertz region with geometries that can be scaled to meet different resonant frequency requirements in both transmission and reflection modes [16–18]. Their miniaturization capability, spectral versatility, and low power consumption makes metasurfaces a viable candidate for use in THz wireless communication systems. Additionally, metasurfaces can be used in cylindrical setups to achieve cloaking and bend electromagnetic waves around an object or introduce currents for scattering cancelation, therefore making an object invisible from a specific direction [19–21].

In this paper, we explore the use of a flexible metasurface formed from a set of anisotropic c-shape split ring resonators and fabricated using a rapid-prototyping technique known as hot-stamping [22]. Since the hot-stamping technique uses a paper substrate, the metasurface is flexible and can be easily bent to conform to a curved surface. We investigate both experimentally and numerically how this bending affects the transmitted beam's refraction angle. A close agreement between our measurement results and simulation results for a metasurface designed to operate at 200 GHz shows that substrate curvature has little effect on the direction of the beam emerging from the metasurface. This result confirms that phase gradient metasurfaces created with hot-stamping can be employed on curved surfaces without sacrificing performance.

## 2 Meta-element Design

We consider a metasurface composed of an array of metallic c-shaped split-ring resonators deposited on a 156-μm thick paper substrate with a refractive index of 1.5. First, a single resonator was designed to have a resonance at approximately 200 GHz. The c-shaped resonator is one of the commonly used resonator designs for terahertz metamaterials due to the simplicity and wide range of possible responses [23, 24]. The geometry is defined in Fig. 1a. The resonator has an outer radius of 233 μm, an opening angle of 45°, and a metallic width of 40 μm. The unit cell period is 680 μm. To verify that the meta-element correctly produces a

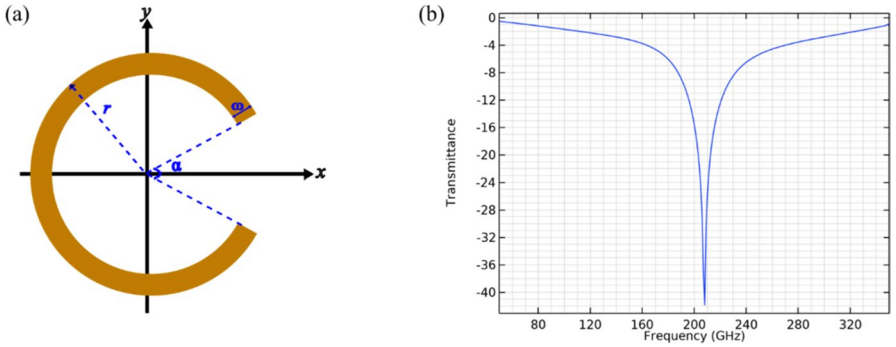


**Fig. 1** **a** Schematic of single c-shape split ring resonator with outer radius $r = 233$ μm, sector angle $\alpha = 45°$, and metallic width $\omega = 40$ μm. **b** Simulated transmittance of an infinite array of identical c-shape resonators, showing a pronounced resonance at 207 GHz

resonant frequency at approximately 200 GHz, we use a finite element method (FEM) simulation. We excite the metasurface array with a plane wave with an electric field at normal incidence along $x$, and we extract the response in the same polarization, $x$ (co-polarization geometry). Figure 1b shows the simulated transmission spectra through a periodic array of the unit cell, indicating a strong resonance at 207 GHz for the chosen geometrical parameters.

Next, we realize a variety of amplitude and phase responses by changing the geometrical parameters of the resonator. We simulate over 3500 resonators, changing the values of the outer radius and opening angles. Figure 2 shows the resulting amplitude and phase transmission of the cross-polarized field, at a frequency of 200 GHz, for one particular orientation of the resonator. As can be seen, we can vary the amplitude transmission from 20 to 50% of the incident beam and cover the complete phase range from $-\pi$ to $+\pi$. Of note, it is possible to select a set of designs for which the amplitude transmission is constant

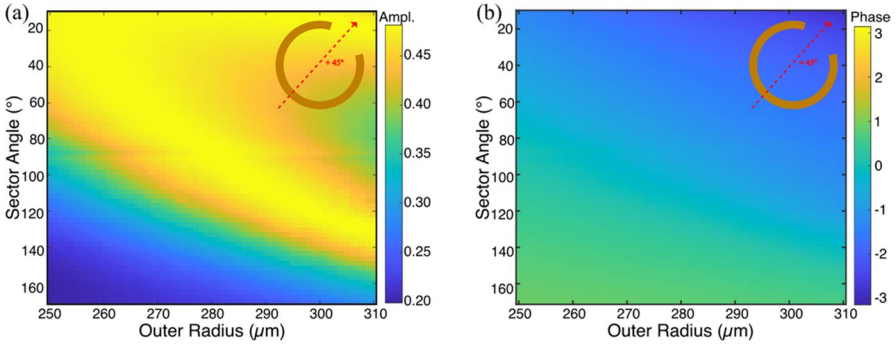


**Fig. 2** A large number of c-shape split ring resonators was simulated with various outer radius and sector angle combinations. **a** Simulated amplitude results of c-shape split ring resonator rotated + 45° from the $x$-axis. **b** Simulated phase response of c-shape split ring resonator rotated + 45° from the $x$-axis

(approximately 0.45), but the phase varies over the full 2 $\pi$ range. We can exploit this phase-only modulation, as described below.

## 3 Metasurface Beam Steering

With the results of Fig. 2, we can realize a variety of amplitude and phase profiles. In the following, we consider the example of cross-polarized beam-steering in a transmission geometry. Electromagnetic wave incident on a metasurface follows the generalized Snell's law of refraction derived from Fermat's principle [25]. In this study, we consider a linearly polarized terahertz beam that is incident on the metasurface at an angle of $\theta_i$ ($\theta_i = 0$ is normal incidence). The angle of the transmitted refracted beam ($\theta_t$) is obtained from:

$$n_t \sin(\theta_t) - n_i \sin(\theta_i) = \frac{\lambda_0}{2\pi} \frac{d\varphi}{dx} \tag{1}$$

where $n_i$ and $n_t$ are the refractive indices of the surrounding media and $\lambda_0$ is the wavelength of the transmitted beam. When the metasurface is optically thin, it can be treated as an interface and $n_i = \mathrm{n_t}$ [26]. Thus, we use $n_i = \mathrm{n_t} = 1$. In Eq. (1), $d\phi/dx$ is the derivative of the phase across the metasurface, also seen in Fig. 1 of [25]. In our discretized geometry, $d\phi$ is the phase discontinuity between adjacent elements, while $dx = 680\mu\mathrm{m}$ is the unit cell size. We consider an array with a phase gradient chosen such that it produces a refracted beam angle of $\theta_t = 16°$, which corresponds to $d\phi = \pi/4$. From the simulated results shown in Fig. 2, we select eight geometries that all exhibit similar amplitude responses as well as phase differences of $\pi/4$ between each successive element. The eight chosen designs are shown schematically in Fig. 3b. The periodic length and width of each unit cell is $p_x = p_y = 680$ µm. The specific geometry of each unit cell is $r_1 = 310$ µm, $r_2 = 289$ µm, $r_3 = 270$ µm, and $r_4 = 260$ µm with $\alpha = 11°$, 18.9°, 45.5°, and 74.6°, respectively. Unit cells 1 through 4 are rotated +45° about the $x$-axis and unit cells 5 through 8 are mirror symmetries of units 1 through 4 that are rotated −45° about the $x$-axis.

Based on the simulation results of Fig. 2, we fabricate eight metasurfaces consisting of uniform arrays of each of the selected shapes. We use a hot-stamping technique which deposits a thin metal layer on a paper substrate [22]. First, the array is printed onto a piece of white paper using an ordinary laser printer. Then, gold deco foil is transferred onto the paper using a heated laminator. The gold sticks to the printed ink, producing an array of thin metallic split-ring resonators. An example of a printed metasurface is shown in Fig. 3a. Next, these eight metasurfaces are measured individually using a THz time-domain spectroscopy system. The metasurface is placed between the transmitter and receiver, along with two dielectric Teflon lenses each with focal length of 60 mm, producing an intermediate focus with a spot size of roughly 8.0 mm at a frequency of 0.2 THz. The transmitter is oriented to produce horizontally polarized radiation, while the receiver is oriented to detect vertically polarized radiation. We confirmed that, without the metasurface, the detected intensity at 200 GHz is over 400 times smaller than with the metasurface. From these

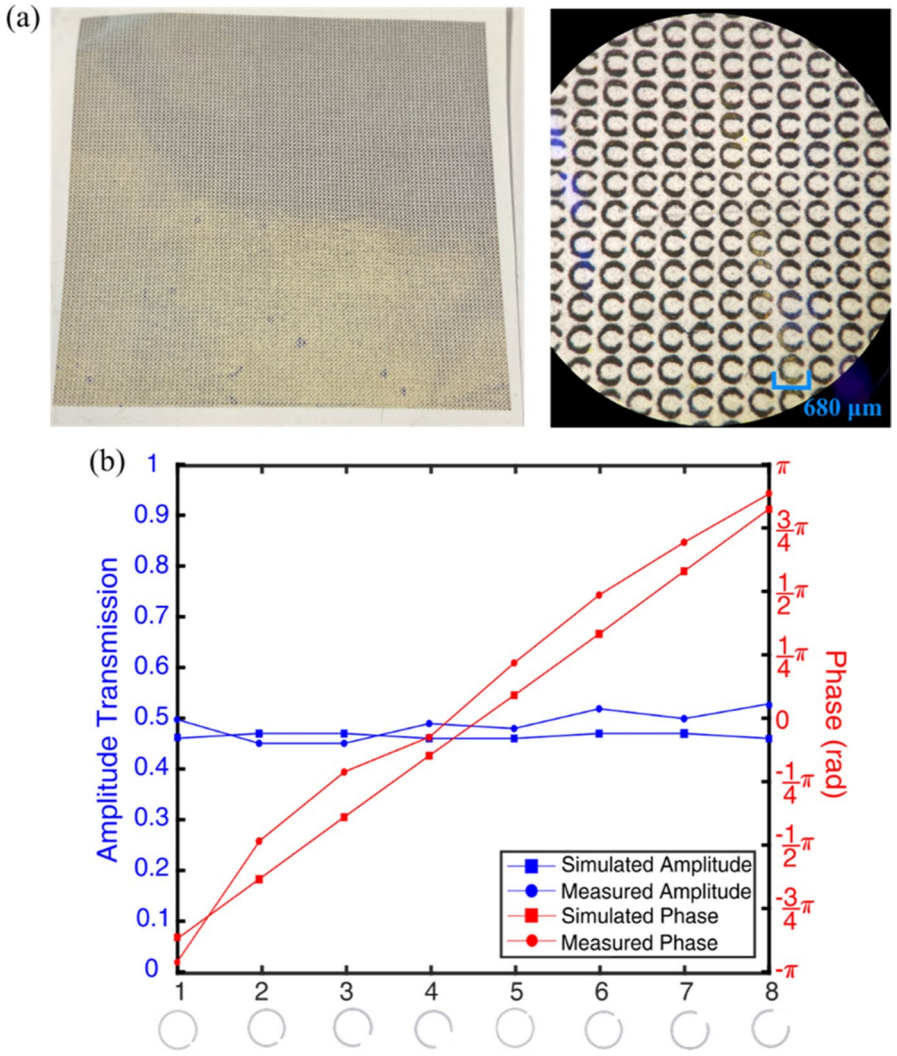


**Fig. 3** **a** Fabricated metasurface of single c-shape resonator with microscopic view. **b** Experimentally measured and simulated phase and amplitude responses of flat metasurfaces corresponding to the indu-vial meta-elements at 200 GHz

measurements, we extract the amplitude and phase responses of the transmitted cross-polarized beam. These measured results are compared with predictions from FEM simulations in Fig. 3b to confirm a constant amplitude of 0.45, and a phase range of 2π with a difference of π/4 between each successive unit cell.

Next, we use the same fabrication technique to create a beam steering metasurface, using the same eight unit cells mentioned earlier. These are arranged in a supercell, such that the phase gradient repeats periodically with a period of $8p_x = 5440$ µm, as shown in Fig. 4. For a flat metasurface, this phase gradient should give rise to a beam deflection of 16°, as noted above. We use this

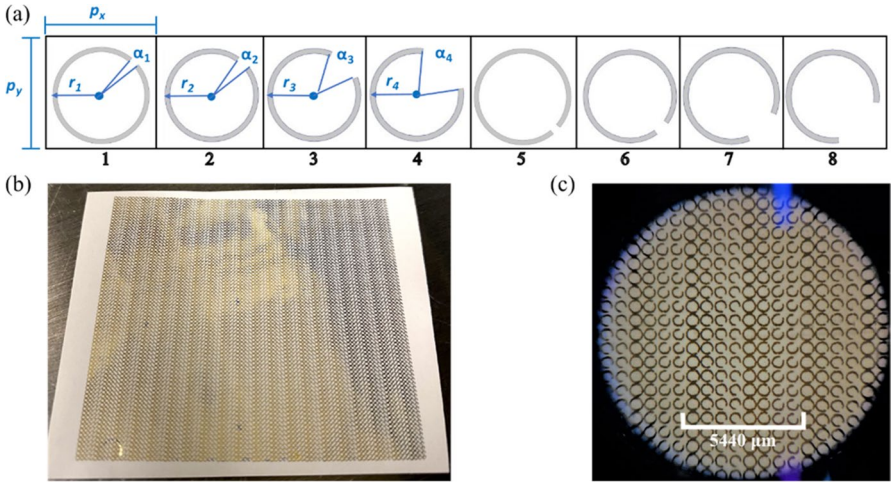


**Fig. 4** **a** Schematic of super cell containing 8 different c-shape split ring resonator geometries. Units 5–8 contain the same geometric parameters as units 1–4, respectively, with rotation of −45° about the *x*-axis instead of +45°. **b** Fabricated flexible metasurface using hotstamping method on a piece of paper with gold deco foil. **c** Microscopic view of the printed metasurface array

metasurface to explore the effect of substrate curvature on this deflection angle, using the same experimental setup.

## 4 Impact of Bending on the Transmitted Beam Angle

To explore the effect of metasurface curvature, we use a series of cylindrical objects of known radius as templates around which the metasurface can be wrapped. In particular, we use four cylindrical objects to curve the substrate around the vertical (*y*) axis as shown in Fig. 5. This results in radii of curvatures of 3.5 cm, 2.6 cm,

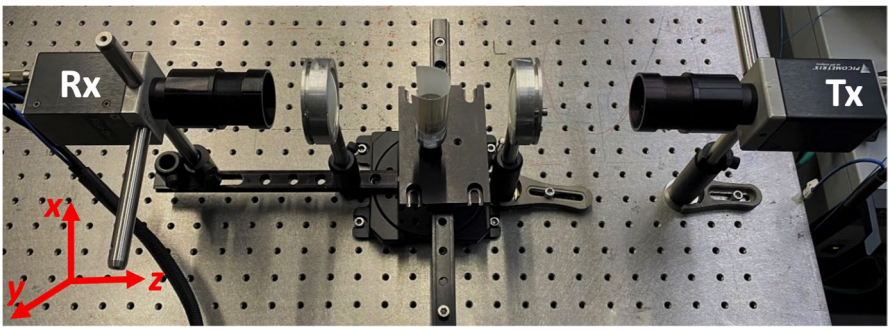


**Fig. 5** Experimental setup using cross-polarization to detect the angle of refraction when the metasurface is bent around a cylinder. In this image, the metasurface is shown with a radius of curvature of 1.2 cm

1.7 cm, and 1.2 cm. As above, the metasurface is placed between the transmitter and receiver, with two lenses to produce an intermediate focus. The transmitter is placed normal to the metasurface (0° incident angle along the $z$-axis). We characterize the transmitted beam as a function of angle, detecting the cross-polarized ($y$) component, by mounting the receiver and 2nd lens on a movable rail that pivots around the illumination point of the curved surface. The receiver is rotated from 0° to 40° to detect the refracted wave in steps of 1°.

In Fig. 6, we display the results of a series of COMSOL simulations of the situations corresponding to the experimental measurements. Because of the curvature, it is not possible to use periodic boundary conditions in these simulations for both dimensions of the metasurface. Therefore, we simulate an entire row of the surface, using periodic boundary conditions only for the dimension parallel to the axis of the cylinder around which the surface is curved (the $y$-axis). In these simulations, a Gaussian beam at 200 GHz is incident on the planar (or curved) surface from the top. The resulting refracted beam emerges from the metasurface, deflected to the left of the normal axis in all cases.

A comparison of our experimental results with these simulations is shown in Fig. 7, comparing the normalized beam profiles for both flat and curved

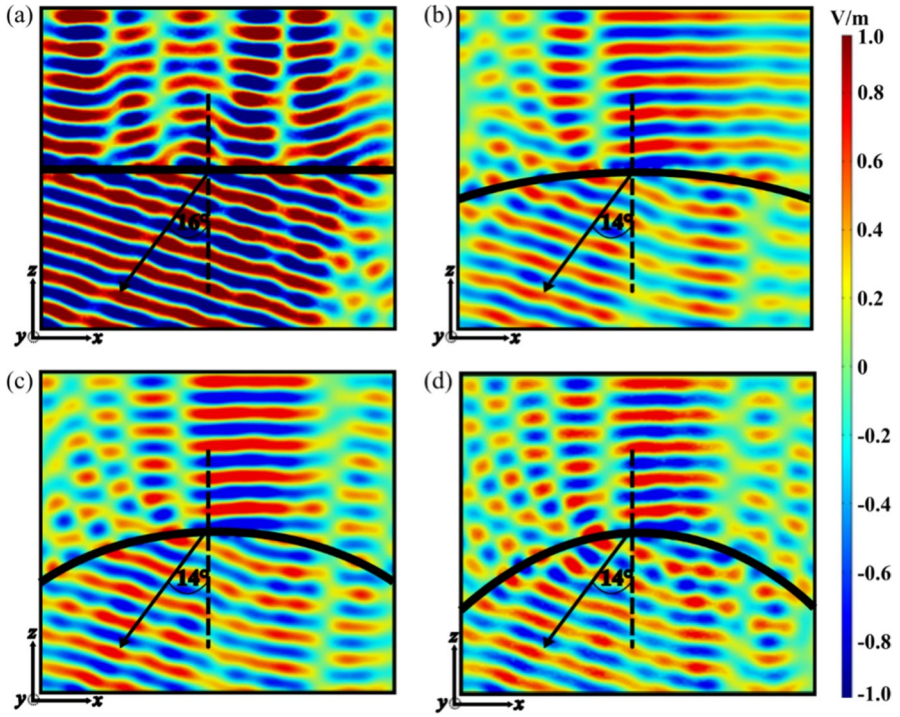


**Fig. 6** Simulation results of the field distributions for transmitted linearly polarized $E_x$ along the propagation direction ($x$–$z$ plane) of the metasurface at 200 GHz when (**a**) flat and (**b**) slightly bent with $r = 3.5$ cm, (**c**) bent with $r = 2.6$ cm, and (**d**) considerably bent with $r = 1.7$ cm

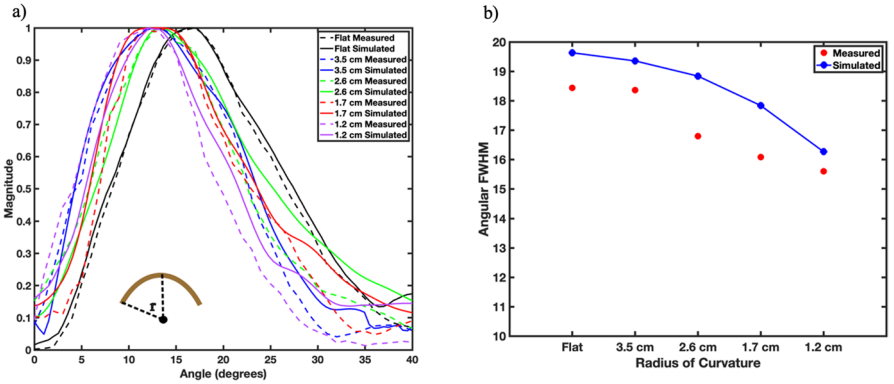


**Fig. 7** **a** Experimentally measured and simulated results of transmitted beam when the metasurface is bent with radius of curvatures, $r = 3.5$ cm, 2.6 cm, 1.7 cm, 1.2 cm, and $\infty$ (flat). **b** Experimentally measured and simulated results of transmitted beam showing the full width at half maximum of the shaped wavefront decreasing as the metasurface curvature increases

metasurfaces at 200 GHz. We observe that in all cases, the center of the diffracted beam is deflected from the normal direction, as a result of the phase gradient of the metasurface. The angle of deflection varies only slightly as the curvature changes, from about 16° when flat to around 13° when most curved. The simulated results (solid curves in Fig. 7a) are in excellent agreement with the measurements. The small observed angular shift is consistent with previous studies [26, 27], and likely results from the fact that a portion of the incident beam spot illuminates a region of the surface at a slight angle, violating the normal incidence condition and changing the transmitted angle according to Eq. (1) above. Figure 7b shows the evolution of the width of the beam (FWHM) at the measurement location, as a function of metasurface curvature. We observe that the diffracted beam becomes slightly narrower, resulting from a small focusing effect associated with the fact that the curved diffracting surface produces a slightly curved wavefront, as a lens. This small wavefront curvature is visible in the simulations shown in Fig. 6, and even more evident when we extract from these simulations the angular width of the beam, as shown in Fig. 7b in comparison with the measured widths.

## 5 Conclusion

We describe a characterization of a flexible phase-gradient metasurface designed to produce a beam deflection at 200 GHz. We study the behavior of this metasurface as a function of its radius of curvature, to explore the implementation of THz metasurfaces on curved surfaces. We find that, within the range of curvatures explored here (where the radius R is always much larger than the meta-atom

size), the angle of the refracted beam does not vary appreciably. A small focusing effect resulting from the curvature of the surface may need to be considered in future implementations of metasurfaces in conformal geometries. Our results are in good agreement with numerical simulations.

**Author Contribution** Y.S. conceptualized and performed the experiments with input and assistance from H.G. Y.S wrote the main manuscript text and prepared figures. H.G and D.M edited the manuscript. The project was supervised by D.M. All authors contributed ideas, discussed the results, and approved the final version of the paper.

**Funding** This work has been funded in part by the US National Science Foundation (CNS-1954780, CNS-2211616) and by the Air Force Office of Scientific Research (FA9550-22–1-0412). Y.S receives partial support from the Science Mathematics and Research for Transformation (SMART) Scholarship program and the Naval Innovative Science and Engineering (NISE) Program.

**Availability of Data and Materials** The datasets used in this study can be accessed by contacting the corresponding author.

## Declarations

**Ethical Approval** Not applicable. No humans or animals were used as test subjects.

**Competing Interests** The authors declare no competing interests.



## References

1. R. Degl'innocenti, H. Lin, M. Navarro-Cía, Nanophotonics **11**(8), 1485–1514 (2022).
2. L. Zhang, X. Pang, S. Jia, S. Wang, and X. Yu, IEEE Communications Magazine, **58**(11), 34–40 (2020).
3. T. Nagatsuma, G. Ducournau, and C. Renaud, Nature Photonics, **10**, 371–379 (2016).
4. H. Elayan, O. Amin, B. Shihada, R.M. Shubair, and M.S. Alouini, IEEE Open J. of the Communications Society, **1**, 1–32 (2020).
5. H. Zeng, S. Gong, L. Wang, T. Zhou, Y. Zhang, F. Lan, X. Cong, L. Wang, T. Song, Y. Zhao, Z. Yang, and D.M. Mittleman, Nanophotonics, **11**(3), 415–437 (2022).
6. G.A. Siles, J.M. Riera, and P. García-Del-Pino, IEEE Antennas and Propagation Magazine, **57**(1), 48–61 (2015).
7. J. Federici and L. Moeller, J. Applied Physics, **107**, 111101 (2010).
8. S. Koenig, D. Lopez-Diaz, J. Antes, F. Boes, R. Henneberger, A. Leuther, A. Tessmann, R. Schmogrow, D. Hillerkuss, R. Palmer, T. Zwick, C. Koos, W. Freude, O. Ambacher, J. Leuthold, and I. Kallfass, Nature Photonics, **7**, 977–981 (2013).
9. J. Ma, R. Shrestha, J. Adelberg, C. Yeh, Z. Hossain, E. Knightly, J. Miquel Jornet and D. Mittleman, Nature, **563**, 89–93 (2018).

10. J.M. Jornet, E.W. Knightly, and D.M. Mittleman, Nature Communications, **14**(1), 841 (2023).
11. Z. Shaikhanov, F. Hassan, H. Guerboukha, D.M. Mittleman, and E.W. Knightly, Proceedings of the 15th ACM Conference on Security and Privacy in Wireless and Mobile Networks, (2022).
12. X. Cai, R. Tang, H. Zhou, Q. Li, S. Ma, D. Wang, T. Liu, X. Ling, W. Tan, Q. He, S. Xiao, and L. Zhou, Advanced Photonics, **3**(3), (2021).
13. D. Headland, T. Niu, E. Carrasco, D. Abbott, S. Sriram, M. Bhaskaran, C. Fumeaux, and W. Withayachumnankul, IEEE J. of Selected Topics in Quantum Electronics, **23**(4), (2017).
14. V. Su, C. Chu, G. Sun, D.P. Tsai, Optics Express, **26**, 13148-13182 (2018).
15. M. Khorasaninejad, W.T. Chen, R.C Devlin, J. Oh, A. Y. Zhu, and F. Capasso, Science, **352**, 1190–1194 (2016).
16. H.T. Chen, W.J. Padilla, J.M. Zide, A.C. Gossard, A.J. Taylor, and R.D. Averitt, Nature, **444**, 597–600 (2006).
17. H.T. Chen, J.F. O'Hara, A.K. Azad, A.J. Taylor, R.D. Averitt, D.B. Shrekenhamer, and W.J. Padilla, Nature Photonics **2**, 295–298 (2008).
18. H.T. Chen, W.J. Padilla, M.J. Cich, A.K. Azad, R.D. Averitt, and A.J. Taylor, Nature Photonics, **3**, 148–151 (2009).
19. C. Valagiannopoulos and A. Sihvola, Journal of Optics, **23**, 15609 (2021).
20. C. Y. Tay and Z. N. Chen, IEEE Transactions on Antennas and Propagation, **69**, 254 (2021).
21. D. L. Sounas, R. Fleury, and A. Alu, Physical Review Applied, **4**, 014005 (2015).
22. H. Guerboukha, Y. Amarasinghe, R. Shrestha, A. Pizzuto, and D.M. Mittleman, Optics Express, **29**, 13806-13814 (2021).
23. A. K. Azad, J. Dai, and W. Zhang, Optics Letters, **31**, 534 (2006).
24. X. Zhang, Z. Tian, W. Yue, J. Gu, S. Zhang, J. Han, and W. Zhang, Advanced Materials, **25**(33), 4567–4572 (2013).
25. N. Yu, P. Genevet, M.A. Kats, F. Aieta, J.P. Tetienne, F. Capasso, and Z. Gaburro, Science, **334**, 333–337 (2011).
26. Y. Xie, C. Yang, Y. Wang, Y. Shen, X. Deng, B. Zhou, and J. Cao, Scientific Reports, **9**(1), 1-8 (2019).
27. N. Han, L. Huang, and Y. Wang, Optics Express, **26**(24), 31625 (2018).